remote sensing

MDPI

Article

Prediction of Species-Specific Volume Using Different Inventory Approaches by Fusing Airborne Laser Scanning and Hyperspectral Data

Kaja Kandare [1,2,*], Michele Dalponte [3], Hans Ole Ørka [2], Lorenzo Frizzera [3] and Erik Næsset [2]

1 FoxLab, Joint CNR-FEM Initiative, Fondazione E. Mach, Via E. Mach 1, 38010 San Michele all'Adige (TN), Italy
2 Faculty of Environmental Sciences and Natural Resource Management, Norwegian University of Life Sciences, P.O. Box 5003, N-1432 Ås, Norway; hans-ole.orka@nmbu.no (H.O.Ø.); erik.naesset@nmbu.no (E.N.)
3 Department of Sustainable Agro-Ecosystems and Bioresources, Research and Innovation Centre, Fondazione E. Mach, Via E. Mach 1, 38010 San Michele all'Adige (TN), Italy; michele.dalponte@fmach.it (M.D.); lorenzo.frizzera@fmach.it (L.F.)
* Correspondence: kaja.kandare@fmach.it; Tel.: +386-41-292-200

Academic Editors: Jixian Zhang, Jixian Zhang, Lars T. Waser and Prasad S. Thenkabail
Received: 16 February 2017; Accepted: 21 April 2017; Published: 26 April 2017

Abstract: Fusion of ALS and hyperspectral data can offer a powerful basis for the discrimination of tree species and enables an accurate prediction of species-specific attributes. In this study, the fused airborne laser scanning (ALS) data and hyperspectral images were used to model and predict the total and species-specific volumes based on three forest inventory approaches, namely the individual tree crown (ITC) approach, the semi-ITC approach, and the area-based approach (ABA). The performances of these inventory approaches were analyzed and compared at the plot level in a complex Alpine forest in Italy. For the ITC and semi-ITC approaches, an ITC delineation algorithm was applied. With the ITC approach, the species-specific volumes were predicted with allometric models for each crown segment and aggregated to the total volume. For the semi-ITC and ABA, a multivariate *k*-most similar neighbor method was applied to simultaneously predict the total and species-specific volumes using leave-one-out cross-validation at the plot level. In both methods, the ALS and hyperspectral variables were important for volume modeling. The total volume of the ITC, semi-ITC, and ABA resulted in relative root mean square errors (RMSEs) of 25.31%, 17.41%, 30.95% of the mean and systematic errors (mean differences) of 21.59%, −0.27%, and −2.69% of the mean, respectively. The ITC approach achieved high accuracies but large systematic errors for minority species. For majority species, the semi-ITC performed slightly better compared to the ABA, resulting in higher accuracies and smaller systematic errors. The results indicated that the semi-ITC outperformed the two other inventory approaches. To conclude, we suggest that the semi-ITC method is further tested and assessed with attention to its potential in operational forestry applications, especially in cases for which accurate species-specific forest biophysical attributes are needed.

Keywords: species-specific volume; semi-individual tree crown; individual tree crown; area-based approach; *k*-MSN; airborne laser scanning; hyperspectral data; data fusion; forestry

1. Introduction

Stem volume is one of the most relevant resource attributes of forest inventories. In most European countries, volume is usually estimated or modeled based on field measurements [1]. In the Nordic countries, conventional forest inventories at various geographical scales have over the past few decades been enhanced by using remotely sensed data such as airborne laser scanning (ALS) and stereo aerial photography [2,3]. It has been shown that for local management planning, data from ALS may reduce

the overall costs by reducing the economic losses caused by incorrect decisions due to erroneous data [4]. One of the biggest challenges in remote sensing-assisted inventories is the discrimination among tree species [5]. Moreover, combining ALS data with hyperspectral images may improve the accuracy of species identification [6]. The tree species information is needed for many forest applications, especially to retrieve species-specific forest biophysical properties, such as volume and diameter at breast height (DBH), to derive biodiversity indicators and to plan silvicultural activities and cutting regimes.

Due to accurate three-dimensional measurements obtained by ALS [7,8], the ALS technology has become one of the most valuable remote sensing methods for providing forest information. By using ALS data, biophysical attributes such as volume, height, DBH, crown area, and stem density can be derived or modeled with high accuracies [2,9–12]. However, the estimation of biophysical attributes can be challenging in dense, multispecies, heterogeneous forest stands [13,14]. In the past, ALS data were examined to classify the tree species at the individual tree crown (ITC) level using shape, structure, and intensity features of the tree crowns [5,15]. In addition, when species-specific biophysical attributes are required, ALS data are often fused with optical images, i.e., color-infrared [16–18], multispectral [19,20], or hyperspectral [21,22] images, in order to improve the tree species classification [6,23,24]. Recently, multi- or hyper-spectral ALS sensors were developed with a high potential to be used as a future single-sensor solution for forest mapping [25–27]. Currently, remotely sensed hyperspectral data are the most promising data source for classifying tree species due to their ability to detect subtle variations in the chemical and structural properties of the tree canopy. Likewise, other studies demonstrated the success of identifying tree species in other ecosystems [28,29]. Thus, the remote sensing technologies that currently are considered to have the greatest potential to improve forest attribute characterization are ALS, describing the 3D forest structure, and hyperspectral imagery, outperforming other techniques for the identification of tree species [30]. The fusion of both has the potential to improve the forest attribute prediction accuracy [31].

Most local forest management inventories assisted by ALS data follow the area-based approach (ABA). For field sample plots distributed across the area of interest, several variables are extracted from the ALS echoes describing structural properties, for which the statistical relationships with field-measured biophysical attributes are constructed. The relationships, typically in the form of regression models, are then used to predict biophysical attributes for larger areas [9,32]. As an alternative, individual trees can be identified and the forest resource variables can be estimated as an aggregate of individual tree properties. To obtain tree attributes, the ITC approach was introduced [33]. With the ITC approach, crown segments are detected and delineated by applying segmentation algorithms [34,35]. The crown segments, often referred to as ITCs, can contain none, one, or several trees. In particular, this approach presumes that one crown segment contains exclusively one tree. For each crown segment, various ALS-derived structural variables are extracted, such as height and crown area. Based on these variables, the biophysical attributes, such as volume and DBH, are predicted for each segment and can be aggregated to other scales, e.g., a forest stand. Detection errors, i.e., omission error (failure to detect a tree or segmenting multiple trees into a single crown segment) and commission error (detecting an object that is not a tree or splitting a single tree into multiple crown segments), usually lead to underprediction of the forest biophysical attributes [36]. To overcome this problem, the semi-ITC approach has been proposed [37], which, in contrast to the ITC approach, allows a crown segment to contain multiple trees.

Several studies in Finland aimed to estimate species-specific forest volume using the combination of ALS data and aerial imagery based on ABA for three species groups: Norway spruce, Scots pine, and deciduous [16–18,38]. All these studies used a non-parametric *k*-most similar neighbor (*k*MSN) approach [39] based on Packalén and Maltamo [16]. Packalén and Maltamo [16] compared two approaches for determining species-specific volumes at the plot level. The first approach predicted the total volume using ALS data, upon which the species-specific volume was obtained by multiplying the total volume by the proportion of each tree species obtained from aerial photographs and fuzzy

classification. The second approach used the *k*MSN method for simultaneous prediction of volumes by tree species. The *k*MSN method resulted in more accurate species-specific volume estimates, except for the total volume where the fuzzy classification performed slightly better. Packalén and Maltamo [17] extended the *k*MSN approach from the previous study [16] to a stand level and tested the simultaneous prediction of volume, stem number, basal area, basal area median diameter, and tree height for the same tree species groups. The attributes of coniferous tree species were predicted accurately and those of deciduous trees less accurately, since they were minority species. Vauhkonen et al. [38] tested the performance of alpha shape metrics calculated from ALS data combined with image variables for species-specific volume predictions at the plot level. They demonstrated that using only ALS variables resulted in less accurate estimates compared to using combined ALS and images variables. Niska et al. [18] compared the *k*MSN method with three artificial neural network modeling methods: the multilayer perceptron (MLP), support vector regression (SVR), and self-organizing map (SOM) at the plot and stand level. The results revealed that the SVR and MLP models reached the greatest prediction accuracy, the *k*MSN a lower accuracy, and the SOM the smallest prediction accuracy. It should be noted that the SVR and MLP yielded negative estimates to some extent, whereas the *k*MSN and SOM estimates were always within the range of the modeling data.

In Norway, Breidenbach et al. [37] determined species-specific volumes for four dominant tree species (spruce, pine, birch, and aspen) using the ABA and semi-ITC approaches, combining the ALS and multispectral data. They applied the *k*NN approach using MSN and random forest (RF) methods for calculating statistical distances between the neighbors. The volumes predicted with the semi-ITC approach resulted in smaller RMSE compared with the ABA results. Ørka et al. [23] evaluated tree species composition in a Norwegian forest using (1) ALS data, (2) multispectral imagery, (3) hyperspectral imagery, (4) fused ALS and multispectral data, and (5) fused ALS and hyperspectral data. Subsequently, they predicted the basal area for spruce, pine, and deciduous trees for three inventory approaches: ABA, semi-ITC, and ITC. For the ABA and semi-ITC approach, the *k*NN algorithm with an Euclidean distance matrix was applied. The results suggested that the greatest species accuracy was achieved by fusing the ALS and hyperspectral data. The ITC approach resulted in the highest accuracy for deciduous species, while the ABA performed the best for the other tree species.

As mentioned above, different remote sensing-assisted forest inventory approaches have been suggested to assess species-specific forest attributes. Each of them has their own pros and cons. The advantage of the ABA is that it provides predictions with small systematic errors, i.e., mean differences, but at the same time only the attributes of the main tree species can be predicted with high accuracy, while for the minority species the errors were large and consequently resulted in inaccurate species-specific attributes [23]. The ITC-based approaches are suitable for developing species-specific models which could lead to more accurate stand-level estimations, particularly for mixed stands. The main drawback of the ITC procedure are the under-predictions due to problems in detecting suppressed and understory trees, especially in stands with a complex forest structure. We expect that a solution for alleviating systematic errors lies in the semi-ITC approach, which has not been sufficiently explored and tested in various forest conditions and ecosystems. In fact, only a few studies have evaluated and compared the results of species-specific volumes and basal areas obtained from different remote sensing-assisted forest inventory approaches [23,37]. In particular, most of these studies were carried out in boreal forest conditions, accounting for spruce, pine, and deciduous tree species groups. Moreover, most of the remote sensing-assisted inventory methods combine ALS data with aerial photogrammetry or multispectral imagery to obtain species-specific volumes. The fusion of complementary data sources, in particular ALS and hyperspectral data, typically result in greater accuracies in contrast to using the respective data separately [6,23,40]. Therefore, the fusion of ALS and hyperspectral data can offer a powerful basis for discriminating tree species and enables an accurate prediction of species-specific attributes. The *k*NN approach has grown in popularity due to its ability to successfully and simultaneously relate multiple forest attributes derived from field observations to remotely sensed data [41]. However, to the very best of our knowledge, there are no studies to date

that have tested the ITC, semi-ITC, and ABA approaches on a comparative basis with emphasis on species-specific volumes.

Thus, the main goal of the present study was to predict and evaluate the species-specific volume in a complex Alpine forest based on fused ALS and airborne hyperspectral data using three remote sensing-assisted forest inventory approaches, i.e., the ITC, semi-ITC, and ABA. The performances of all three inventory approaches were analyzed and compared for the total volume and volume of five species classes.

2. Materials and Methods

2.1. Data Set Description

2.1.1. Study Area

The 32 km^2 study area is located in an Italian Alpine forest in Pellizzano (46°17′22″N, 10°46′05″E), situated in the province of Trento. The altitude of the forest area ranges from 900 to 2200 m above sea level. The forest is dominated by Norway spruce (*Picea abies* (L.) Karst.), with the presence of other coniferous species (e.g., larch (*Larix decidua* Mill.), silver fir (*Abies alba* Mill.)) and broadleaves species (e.g., rowan (*Sorbus aucuparia* L.), aspen (*Populus tremula* L.), silver birch (*Betula pendula* Roth), and sycamore maple (*Acer pseudoplatanus* L.)). At higher altitudes, the forest is sparse, whereas at lower altitudes, the forest structure is more complex, varying from a one- to multi-layer forest with patches of mixed and homogeneous tree species composition. The forest is managed by selective logging focusing on the productive forest area, especially Norway spruce, and trees are harvested according to their stem diameter.

2.1.2. Field Data

Between the summers of 2013 and 2015, 47 circular sample plots were surveyed. The size of the sample plots was 700 m^2. The center location of each plot was determined with global navigation satellite system (GLONASS) measurements, resulting in a positional error of less than 1 m. At each sample plot, the tree locations were recorded as polar coordinates by measuring the azimuth and range to the center of the plot. For all trees within the sample plot, stem diameter at breast height and tree species were recorded. Tree height for randomly selected trees was measured using a Vertex III hypsometer. Tree heights of the remaining trees were predicted with allometric equations [1]. In each sample plot, only trees with a DBH greater than 7.5 cm were considered in the analysis. Dead or damaged trees were also excluded. In total, 1283 field trees were available for the analysis. The tree level and plot level statistics are summarized in Table 1. The tree species observed for the 1283 trees were: 76.5% Norway spruce, 9.0% larch, 6.2% rowan, 1.7% silver fir, 1.5% silver birch, 1.4% sycamore maple, and 3.7% other minority broadleaves. For the following analysis, we grouped tree species into five classes to predict species-specific volumes using the ITC and semi-ITC approaches: Norway spruce, larch, rowan, silver fir, and other broadleaves (silver birch, sycamore maple, and other minority broadleaves). The field statistics for the total and species-specific volumes are represented in Table 2.

2.1.3. ALS and Hyperspectral Data and Pre-Processing

ALS data were acquired with a Riegl LMS-Q680i sensor between the 7th and 9th of September 2012. The flying speed was approximately 51 m s^{-1} at the altitude of 660 m above ground level with the pulse repetition frequency of 400 kHz. For each emitted pulse, up to seven returns were recorded and the mean point density was 48 points m^{-2}. A digital terrain model (DTM) was extracted from the ALS points with a grid of 0.5 m by the vendor. In the preprocessing, underlying DTM elevations were subtracted from the ALS point elevations to convert ALS point elevations to heights above ground. From these ALS points, a raster canopy height model (CHM) of the area was created with the resolution of 0.5 m.

Table 1. Statistics of the field-observed biophysical attributes at the tree and plot level (SD = standard deviation, DBH = diameter at breast height, H = height, BA = basal area, V = volume).

	Biophysical Attributes	Range (Min-Max)	Mean	SD
Tree level	DBH (cm)	8.0–89.0	33.7	19.7
	H (m)	3.50–42.60	22.37	9.90
	BA (m^2)	0.01–0.62	0.08	0.12
	V (m^3)	0.01–9.21	1.54	1.72
Plot level	Mean DBH (cm)	13.5–71.8	38.0	12.8
	Mean H (m)	7.93–37.90	23.92	7.12
	Stem number (ha)	14–1132	386	228
	BA (m^2 ha^{-1})	0.63–85.73	46.26	21.22
	V (m^3 ha^{-1})	2.47–1363.35	590.28	321.76

Table 2. Statistics of the field-observed total and species-specific volumes for five species classes at the plot level.

Field Volume	Mean (m^3 ha^{-1})	SD (m^3 ha^{-1})	Relative SD (m^3 ha^{-1})
Total	590.28	321.76	54.51
Silver fir	34.88	24.85	71.25
Larch	102.37	114.16	111.51
Other broadleaves	9.64	14.47	150.21
Norway spruce	513.40	318.50	62.04
Rowan	3.36	6.98	207.34

Twenty-one hyperspectral images were acquired on the 13th of June 2013 by an AISA Eagle II sensor with a spatial resolution of 1 m. The minimum overlap among the images was 20%. The images consisted of 65 spectral bands between 403.09 nm and 995.31 nm. The hyperspectral strips were mosaicked into one image. For each pixel, the normalized difference vegetation index (NDVI) was computed based on the red and infrared wavelengths of 646.72 nm and 815.27 nm, respectively, and pixels with NDVI below 0.5 were removed in order to reduce noise and shadowing effects. Afterwards, the value of each pixel was normalized with respect to the sum of the values of the same pixel in all the bands to reduce the minor differences in radiance occurring between the different images [42]. The hyperspectral images were orthorectified using ALS data by the data vendor.

2.2. Methodology

2.2.1. Overview

The flowchart for the species-specific volume prediction for the three remote sensing inventory approaches using ALS and hyperspectral data is presented in Figure 1. For the ITC approach, the predicted volumes were summed per plot and scaled to m^3 per hectare, and for the semi-ITC and ABA approaches, the volumes were scaled to per-hectare values before modelling. In the case of the ITC and semi-ITC approaches, ALS and hyperspectral variables were calculated for each crown segment, whereas for the ABA variables, they were calculated for each subsample plot (sample plot halves). In the ITC approach, the tree species and DBH were predicted per segment. Subsequently, the allometric models were applied to predict species-specific volumes, which were summed up to have the total volume. For the semi-ITC approach and the ABA, the total and species-specific volumes were predicted simultaneously by a non-parametric multivariate *k*NN method using leave-one-out (LOO) cross-validation at the plot level.

The basic idea of the *k*NN method is that biophysical attributes within the target data are predicted by imputing them from the *k* nearest neighbors within the reference data. The nearness of neighbors is measured with the distance matrix between predictors (e.g., ALS and hyperspectral variables), which

are known in the reference and target data sets [43]. For the distance matrix, the most similar neighbor (MSN) method was applied, where the nearness of the k-nearest neighbors was defined in terms of weighted Euclidean distance in a conical search space. We chose this distance as from some preliminary analysis it appeared to be the most suitable among the random forest proximity, Euclidean distance, Euclidean distance without normalization, and Mahalanobis distance for this specific problem. Thus, we applied the *k*MSN, which is a particular type of the *k*NN methods. One property of the *k*MSN method is that the predictions are always within the range of the observed distribution. The main advantages of the *k*MSN approach are that the multivariate responses include the simultaneous predictions of the volumes and preserve their complex variance-covariance structure [39], along with their robustness to handle the outliers or extreme values in the data. The main disadvantage is that the *k*MSN approaches normally require a larger number of observations, although some studies have shown that reasonable results can be obtained also with a limited number of sample plots [37,44,45].

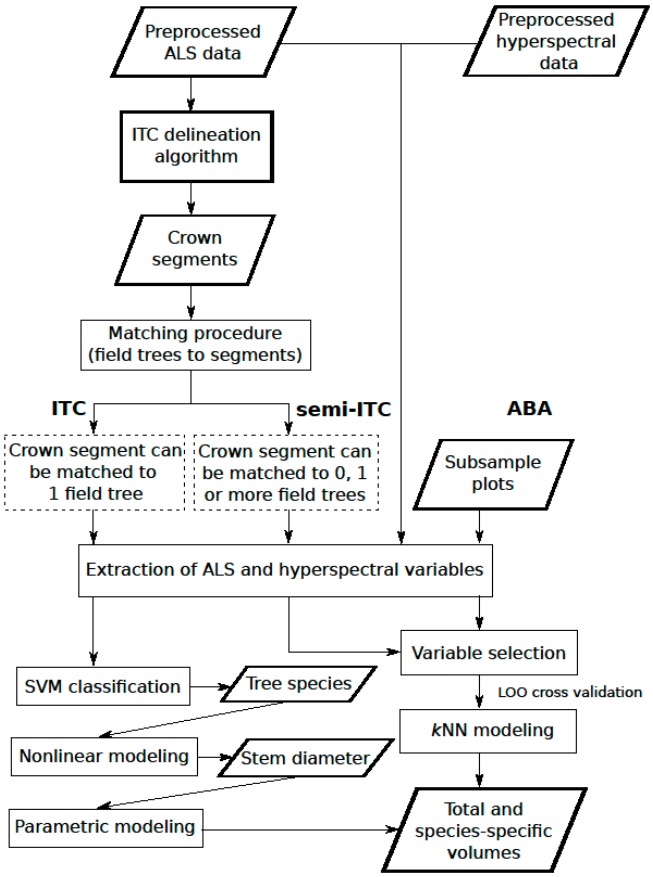

Figure 1. Flowchart of the procedure for predicting total and species-specific volumes.

2.2.2. ITC Delineation Method

To avoid ground hits and effects of rocks and small vegetation, all echoes with the height below 2 m were removed from the point cloud in the preprocessing step. The ITC delineation for the ITC and semi-ITC approaches was conducted with the algorithm implemented in the "itcSegment"-package in the R software [46] based on ALS data. For each crown segment, position, height (h_{max}), and crown area (CA) were calculated. The position and height were determined from the highest ALS point within a crown segment. The crown area (CA) was extracted with the convex hull. The height and crown area were used as ALS variables. The hyperspectral variables were computed for each crown segment as the average value of pixels for all 65 bands, and they are referred to as band means (from $B1$ to $B65$). This step was the same for both the ITC and the semi-ITC approach.

2.2.3. ITC Approach

The ITC approach assumes that each delineated crown segment contains one field tree. The matching procedure of the crown segments and field trees was different from the classical methods [34,47]. An empirical threshold for the permitted distance (horizontal or vertical) between the "matched" crown segment and field tree was avoided. In particular, each segment was matched to the closest field tree according to a 3D distance. To confirm a good match, we fitted a simple linear regression with the field tree height as response (h) and crown segment maximum height as predictor (h_{max}):

$$h_i = b_0 + b_1 \times h_{max_i} + \varepsilon_i, \quad (1)$$

where i corresponds to a crown segment, b_0 and b_1 are fixed parameters, ε_i is the error of tree i ($\varepsilon_i \sim N(0, \sigma^2)$), and σ^2 is the model variance. The prediction interval was defined as:

$$h_i \pm t_{n-p}^{\frac{0.95}{2}} \hat{\sigma} \sqrt{1 + h_{max_i} (X'X)^{-1} h'_{max_i}}, \quad (2)$$

where t stands for the t-distribution, n means a number of segments, p represents a number of model parameters, and X is a design matrix. Out of 629 segments, 25 segments' fitted heights were not within the prediction interval (Figure 2). These 25 segments were excluded from the tree species and stem diameter modeling but not from the accuracy analysis. Breidenbach et al. [37] applied the same procedure to exclude segments with incorrect field trees from modeling. After matching, the ALS and hyperspectral variables were merged for each crown segment.

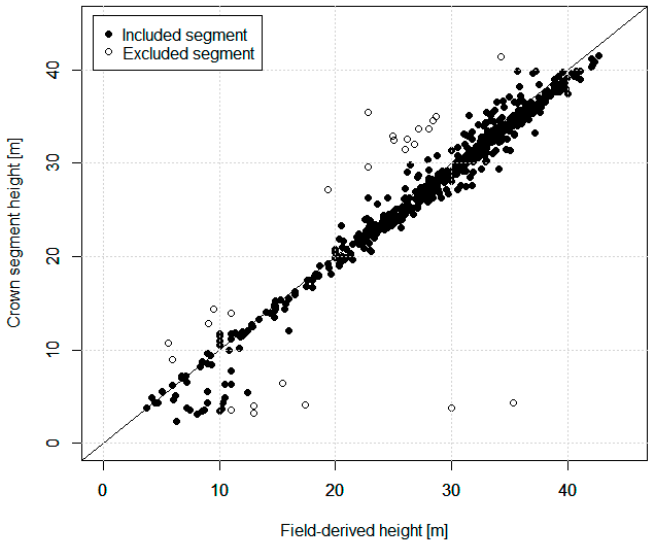

Figure 2. The field-derived tree height of the matched field trees and the respective maximum airborne laser scanning (ALS) height of crown segments.

The tree species were classified at the pixel level with a support vector machine (SVM) classifier using hyperspectral variables. We used the SVM implementation in the R package "kernlab" [48]. The penalty factor (C) was selected with a grid search strategy, testing values of 1, 10, 100, and 1000. The value of 10 turned out to reach the highest classification accuracy. The weights for different species classes were set as a ratio between the number of trees of the most frequent species and the number of trees of each species. The predicted species for each pixel were aggregated within each crown segment according to a majority rule.

The stem diameter at breast height (cm) was predicted for each crown segment using a nonlinear regression model, taken from the study of Dalponte and Coomes [49] conducted on the same dataset. The fitted species-specific nonlinear model was:

$$DBH_{ij} = \varepsilon_j \times {h_{max_{ij}}}^{\rho_j} \times \left(1 + \vartheta_j CA_{ij}\right) \quad (3)$$

where $h_{max_{ij}}$ is the maximum crown segment height (m), CA_{ij} is the crown area (m), and ε_j, ρ_j and ϑ_j are parameters determined in [49]. Indices i and j correspond to segment and species, respectively. Knowing the predicted species and stem diameter, the species-specific volumes were predicted based on allometric models for temperate species of Scrinzi et al. [1]:

$$\hat{V}_{ij} = a_j \times \left(D\hat{B}H_{ij} - d_j\right)^{b_j} \times \left(h_{max_{ij}}\right)^{c_j}, \quad (4)$$

where a_j, b_j, c_j, and d_j are parameters taken from species-specific tables derived from trees in the Trentino province [1]. Finally, the volume was summarized for each species at the plot level.

2.2.4. Semi-ITC Approach

The semi-ITC approach presumes that a crown segment can contain none, one, or more field trees. Thus, each field tree was matched to the closest segment according to a 3D distance. The field derived values of the total and species-specific volumes were assigned to each segment. For the segments that were matched with more than one field tree, the tree volumes were summed up over the total and species-specific volumes. The segments with no match had zero values for all volumes. In the following analysis, all the segments were used for the modelling and accuracy analysis.

The *k*MSN prediction method, implemented in the R package "yaimpute" [50], was applied using the total and species-specific volumes per segment derived from the field observations as response variables and the selected predictor variables per segment derived from the ALS and hyperspectral variables as covariates. The predictor variables were selected with the variable selection method *varSelection* implemented in the R package "yaimpute" [50]. For the selection, the remotely sensed variables were added to the *k*MSN model based on the computed generalized root mean square distance (grmsd) between the predicted and observed response variables among the field observations. The grmsd computes the root mean square distance between the observed and predicted volumes over several variables simultaneously. The variable that was related to the largest grmsd was removed. Finally, the selected predictor variables were: CA, h_{max}, $B4$ (428.96 nm), $B13$ (509.16 nm), $B14$ (518.10 nm), $B29$ (655.98 nm), $B31$ (674.49 nm), $B33$ (693.00 nm), and $B43$ (786.82 nm). The number of the nearest neighbors was selected empirically and the distance to the nearest neighbors, i.e., crown segments, was defined by the MSN distance matrix based on the predictor variables.

2.2.5. ABA

In order to increase the number of plots, i.e., neighbors, important for the *k*MSN method, we subdivided the 47 sample plots into halves, resulting in 94 subsample plots with a size of 350 m^2. The same procedure was applied by Breidenbach et al. [37]. The ALS canopy height- and density-related variables calculated for each subsample plot were the ones also used in other studies [9,23], using the lower limit of the canopy defined by a threshold value of 2 m [9,51,52]. The ALS variables were computed for the first, intermediates, and last returned laser pulses, denoted x, from 1 to 3, respectively: maximum ($h_{\max\_x}$), mean (h_{mean_x}), skewness (h_{sk_x}), kurtosis (h_{ku_x}), and coefficient of variation (h_{cv_x}) of the ALS heights (m) and quantiles corresponding to the 0, 10, 20,...,90 percentiles of the ALS heights ($h_{q10\_x} - h_{q90\_x}$). Furthermore, 10 vertical slices of equal height were defined as a range between the lowest laser canopy height (2 m) and the 90th percentile of the canopy height. Then, the canopy density variables ($d_{1\_x} - d_{10\_x}$) were calculated as the proportions of laser pulses above each vertical slice to the total number of pulses. Additionally, the canopy volume (C_{Vol}) was calculated as the cell-wise difference between rasterized height values (m) of the first (F_{ij}) and last (L_{ij}) returned pulses of the i-th pixel in the j-th sample plot as $C_{Vol} = \sum_j^J (F_{ij} - L_{ij}) \times length(F_{ij})$. The hyperspectral variables were the same as for the semi-ITC. Additionally, the NDVI and the difference vegetation

index (DVI) were computed for each plot as both indices can be potentially good explanatory variables for the volume prediction [53,54].

The variable selection and prediction method employed were the same as for the semi-ITC approach. For the simultaneous volumes prediction, 18 variables were selected: h_{CV_2}, h_{max_1}, h_{q20_1}, h_{q50_1}, h_{q10_2}, h_{q40_2}, h_{q20_3}, h_{q30_3}, d_{10_2}, d_{4_3}, $B3$ (420.34 nm), $B14$ (518.10 nm), $B16$ (535.98 nm), $B20$ (572.65 nm), $B27$ (637.47 nm), $B35$ (711.62 nm), $B38$ (739.59 nm), and $B54$ (891.00 nm). To avoid overfitting, the number of variables should be smaller than the number of samples. In addition, adding more predictor variables in the training data does not always improve the *k*NN model accuracy [55]. Then, we applied the *k*MSN distance metric to find the reference plots for the target plots based on the selected variables above. The number of the nearest neighbors used was based on preliminary tests according to the balance between the highest accuracy and the smallest systematic error.

2.2.6. Accuracy Assessment

For the ITC approach, the tree species classification accuracy was validated at the ITC-level with a 3-fold cross-validation using the overall accuracy (OA), kappa coefficient (KA), the producer's and user's accuracies derived from the confusion matrix. The accuracy of the predicted stem diameter at the ITC-level was assessed with the root mean square error (RMSE), and the mean differences (MD) as an indicator of the systematic error were calculated as

$$RMSE = \sqrt{\frac{\sum_{i=1}^{n}\left(observed_{ij} - predicted_{ij}\right)^2}{n}}, \quad (5)$$

$$MD = \frac{\sum_{i=1}^{n}\left(observed_{ij} - predicted_{ij}\right)}{n} \quad (6)$$

where n is the sample size (number of segments) and i denotes a segment for which the observed and predicted attributes for the j-th species class were calculated. The relative RMSE and MD were calculated by dividing with the mean of the observed values. Additionally, the squared correlation (r^2) was computed as the Pearson's correlation coefficient of observed and predicted values. The accuracy and the systematic error of the total and species-specific volume models at the plot level were calculated with the same statistics as above, where the sample size represented the number of sample plots and i denoted the plot.

The reliability of the predicted volumes by the semi-ITC and ABA was tested by means of LOO cross-validation. For the semi-ITC and ABA approaches, the crown segments and subsample plots, respectively, belonging to the same sample plot, were subsequently left out in the cross-validation process. The accuracies of the predicted total and species-specific volumes at the plot level by both approaches were evaluated with the same measures as for the ITC approach. We performed the Wilcoxon signed rank test to test if the differences between the observed and predicted volumes for all inventory approaches were significantly different at a significance level of 0.05. The Friedman test at the same significance level was applied to check the significance of the differences in the distribution of the differences between the observed and predicted species-specific volumes among sample plots for the three inventory approaches. In addition, we conducted Conover post-hoc analysis in order to decide which pairs of the three inventory approaches were significantly different from each other for each species class volume.

3. Results

3.1. ITC Approach

The ITC segmentation method delineated 629 segments within the 47 plots. The omission and commission errors were 51% and 4%, respectively. When calculating hyperspectral variables per crown, one crown was removed due to the effects from shadowing. Thus, the following analysis comprised

628 crown segments. The tree species overall and kappa accuracies were 85.2% and 0.57, respectively, where the producer's and user's accuracies are shown in Table 3. The predicted stem diameter per each crown segment resulted in an RMSE of 11.0 cm (relative RMSE = 23.40%) and MD of 0.43 cm (relative MD = 0.92%) with the explained proportion of the variance of 0.61. Knowing the predicted species, the species-specific volumes were predicted and aggregated at the plot level (Table 4 and Figure 3). We also checked if the RMSE of the predicted volumes were within the standard deviation of the field volumes (Table 2). In this regard, the RMSEs of the volumes for larch, Norway spruce, and rowan classes were within the standard deviation of the observed volumes while the volumes of the species classes other broadleaves and silver fir were not. Moreover, the Wilcoxon signed rank test showed that the volume differences between the observations and predictions were statistically different for all species classes ($p \leq 0.05$), except for the larch and rowan classes.

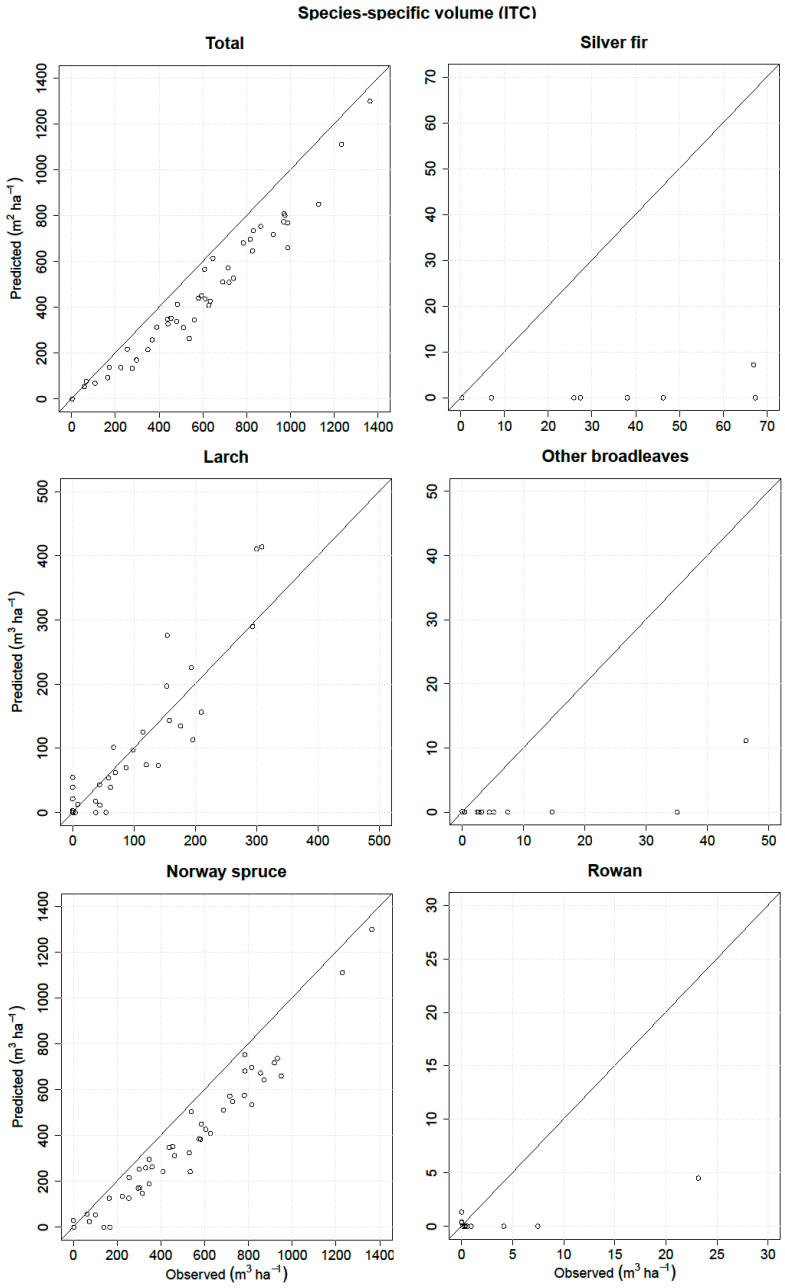

Figure 3. Observed versus predicted total and species-specific volumes at the plot level derived from the individual tree crown (ITC) method.

Table 3. Producer's and user's accuracies of tree species classification at the ITC level.

	Silver Fir	Larch	Other Broad Leaves	Norway Spruce	Rowan
Producer's accuracy (%)	16.7	71.6	14.3	90.1	75.0
User's accuracy (%)	100	58.1	50.0	92.2	81.8

Table 4. Results of the predicted volumes derived from the ITC approach, aggregated to the plot level (* = differences between the predicted and observed volumes are significantly different from zero ($p \leq 0.05$), RMSE = root mean square error, and MD = mean differences).

Volume	RMSE (m^3 ha^{-1})	Relative RMSE (%)	MD (m^3 ha^{-1})	Relative MD (%)	r^2
Total	152.18	25.78	132.37	22.43 *	0.95
Silver fir	40.53	116.2	33.98	97.41 *	0.27
Larch	48.7	47.57	−5.29	−5.17	0.90
Other broadleaves	14.71	152.67	8.77	91.02 *	0.58
Norway spruce	151.26	29.46	130.34	25.39 *	0.95
Rowan	6.21	184.71	2.77	82.25	0.76

3.2. Semi-ITC Approach

For the semi-ITC approach, the same segmentation method was employed as for the ITC approach, but with different matching procedures where every field tree was matched to the closest segments. Fifty-four segments out of 628 remained without any field match. The number of nearest neighbors was selected empirically, according to the smallest RMSE and MD values. We choose three neighbors, even if two or four revealed similar results. The predicted volumes were aggregated at the plot level (Table 5) and displayed in Figure 4. The highest accuracies were reached for total, Norway spruce, and larch volumes, while the lowest accuracies were obtained for silver fir, other broadleaves, and rowan volumes. The relative RMSE of the predicted silver fir, other broadleaves, and rowan volumes were also greater than the relative standard deviations of the corresponding observed volumes (Table 2). The predicted volumes for total, larch, and Norway spruce resulted in minor systematic errors with relatively high r square correlations, except for larch. All the predicted volumes were underpredicted except for the total and Norway spruce volumes. Regarding the Wilcoxon signed rank statistic, the differences between the observed and predicted volumes were not statistically significant ($p > 0.05$) for all species classes.

Table 5. Results of the predicted volumes derived from the semi-ITC approach extended to the plot level.

Volume	RMSE (m^3 ha^{-1})	Relative RMSE (%)	MD (m^3 ha^{-1})	Relative MD (%)	r^2
Total	102.78	17.41	–1.59	–0.27	0.90
Silver fir	15.35	258.48	1.04	17.5	0.16
Larch	76.02	96.95	5.91	7.54	0.51
Other broadleaves	8.82	330.74	0.41	15.57	0.03
Norway spruce	124.25	24.73	–9.07	–1.81	0.85
Rowan	2.69	341.02	0.11	14.53	0.50

3.3. ABA

The number of nearest neighbors was set to three, although the volumes of the majority species did not substantially change using one or two neighbors. The accuracy assessment and visualization of the volume predictions using the *k*MSN approach appear in Table 6 and Figure 5. The RMSE of the total volume (Table 6) was within the standard deviation of the observed volumes except for the other broadleaves volume. The Wilcoxon signed rank test showed that the differences between the predicted and observed volumes were not statistically significant ($p > 0.05$).

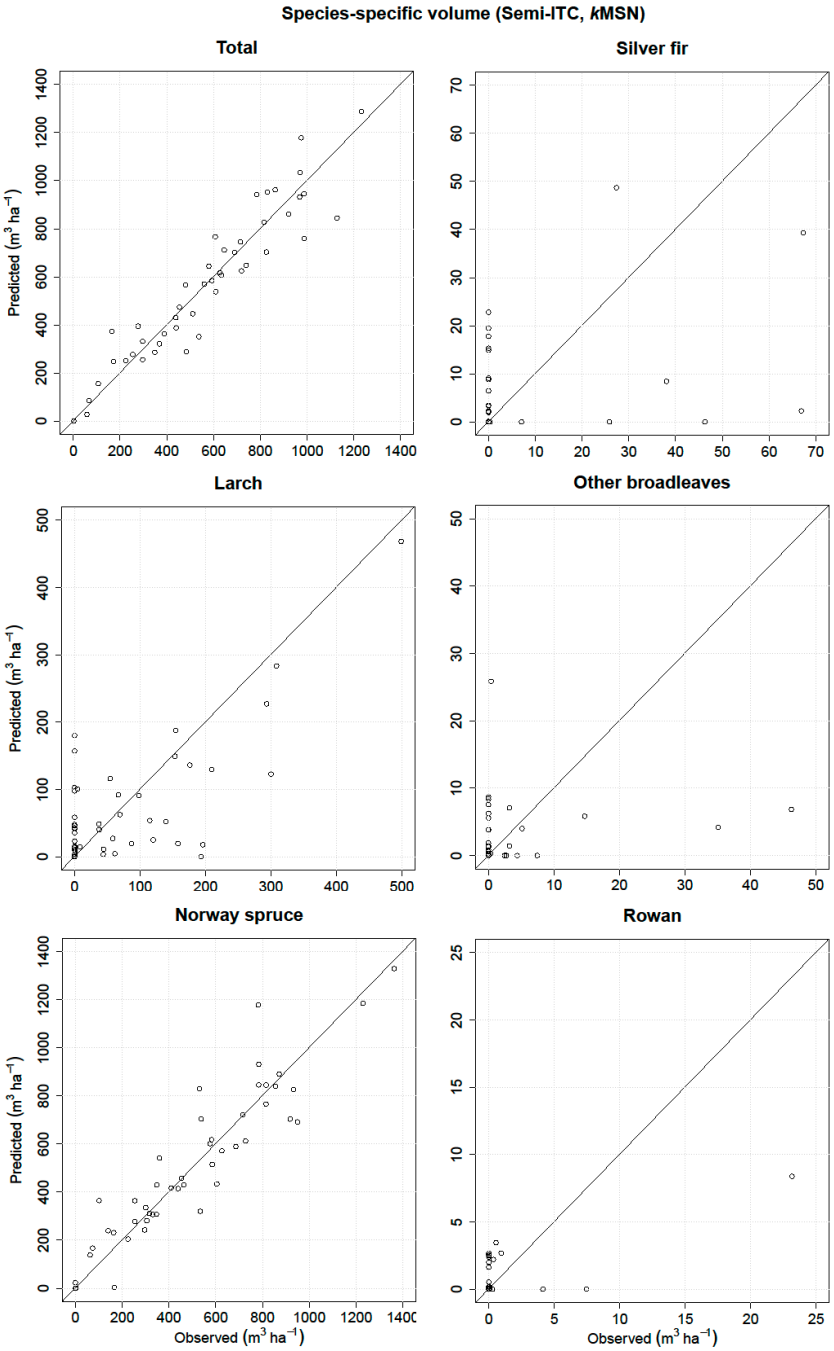

Figure 4. Observed versus predicted species-specific volumes at the plot level derived from the semi-ITC method.

Table 6. Results of the predicted volumes using the k-nearest neighbor approach derived from ABA at the plot level.

Volume	RMSE (m^3 ha^{-1})	Relative RMSE (%)	MD (m^3 ha^{-1})	Relative MD (%)	r^2
Total	182.75	30.95	−15.88	−2.69	0.67
Silver fir	18.01	303.25	−0.49	−8.26	0.01
Larch	69.36	88.44	10.00	12.76	0.60
Other broadleaves	8.20	306.02	1.74	65.02	0.12
Norway spruce	183.54	36.52	−27.77	−5.53	0.68
Rowan	3.76	465.42	0.63	78.56	0

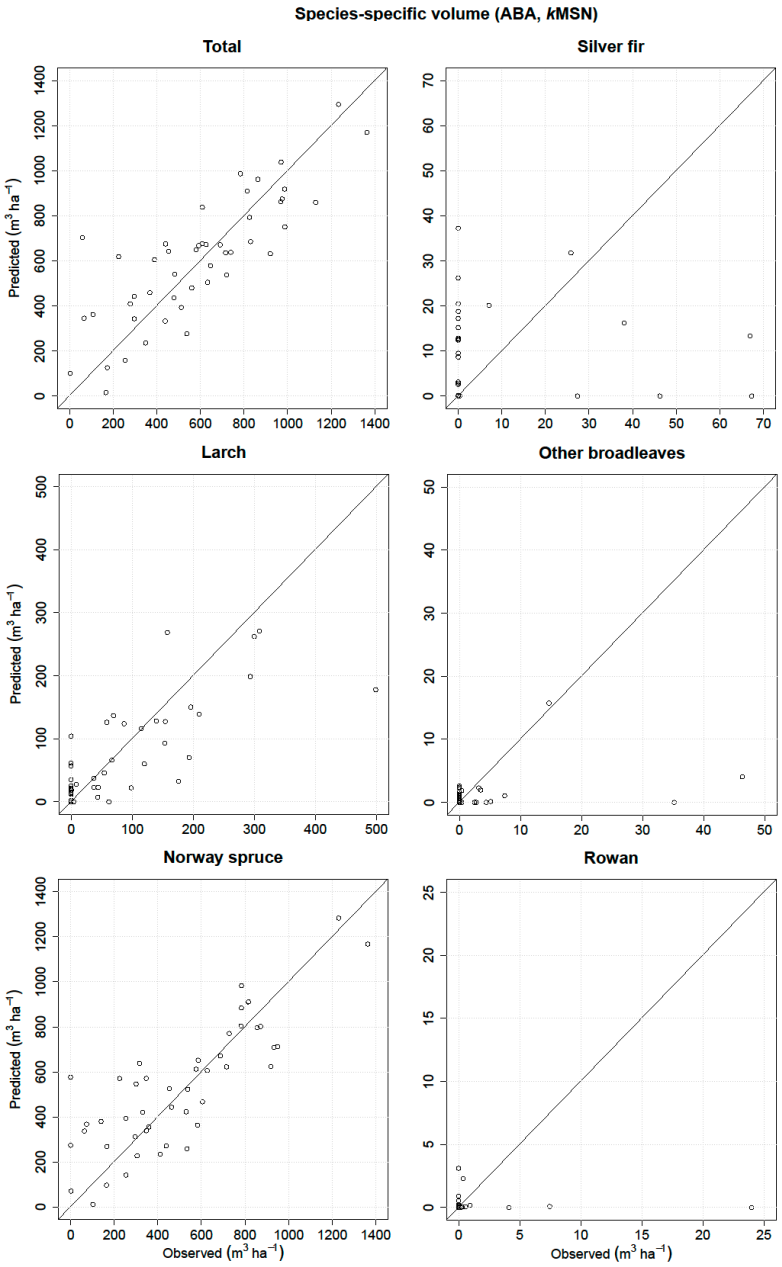

Figure 5. Observed versus predicted species-specific volumes at the plot level derived from the area based approach (ABA) method.

3.4. Comparison of the Different Inventory Approaches

For all three inventory approaches, the RMSEs and MDs of the total and five species-specific volumes were compared (Figure 6). The lowest relative RMSEs of the volumes were achieved by the ITC approach, except for the total and Norway spruce volumes where the semi-ITC resulted in the greatest accuracies. The ABA and semi-ITC approaches resulted in quite large RMSEs for the minority species, like silver fir, rowan, and other broadleaves. The accuracies for the total volume and majority species (Norway spruce) were in the same range for all three inventory approaches. Regarding the relative MDs, the smallest values were obtained by the semi-ITC approach, except for the silver fir which resulted in smaller systematic error by ABA. The ITC approach resulted in the largest MDs, except for the rowan where the ABA resulted in a larger MD. The Friedman test showed that the three inventory approaches had statistically significant different median of the differences between

the observed and predicted volumes per plot for all species classes, except for the larch. Furthermore, we performed post-hoc analysis for the Friedman's Test, which demonstrated that the pairs of the inventory approaches (ITC vs. semi-ITC, ITC vs. ABA, semi-ITC vs. ABA) were significantly different ($p \leq 0.05$) from each other for the total, silver fir, other broadleaves, and rowan volumes. For the pairs of ITC vs. semi-ITC and ITC vs. ABA, the differences between the larch and Norway spruce volumes were also statistically significant but not for the pair of semi-ITC vs. ABA ($p > 0.05$). Overall, the greatest balance between the RMSEs and MDs for all volumes was achieved by the semi-ITC approach.

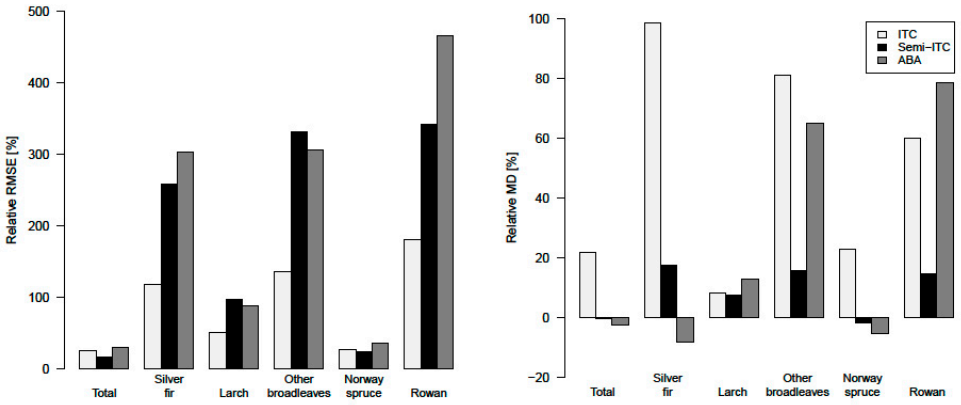

(**a**) (**b**)

Figure 6. (**a**) Relative RMSEs and (**b**) relative MDs of the total and five species classes' volumes obtained by the three inventory approaches: ITC, semi-ITC, and ABA.

4. Discussion

Many methods have been proposed for fusing ALS data with stereo or airborne multispectral or hyperspectral images in order to achieve a more accurate species recognition [23,56,57]. In this study, we showed that the fusion of ALS and hyperspectral data enabled the prediction of volumes at good accuracy levels. Moreover, hyperspectral variables were not only used for species classification, but they were also incorporated in the common ALS framework as they were selected as important variables for volume modeling. At the moment, hyperspectral data are the most powerful tool for species identification [6] and consequently they can improve the accuracy of the predicted biophysical attributes [31]. Forest inventories can be improved by the use of these combined data as they can increase the spatial detail, coverage, and accuracy of forest biophysical attributes. Thus, the combined data also helps forest managers to develop a broad and detailed database of forestry information to be coupled with a decision support system [58].

The accuracies of the species-specific volumes of the minority species obtained by the ITC approach were relatively higher compared to the semi-ITC and ABA approaches, but the accuracies of the more frequent species, i.e., the Norway spruce, were very much alike. The semi-ITC approach had slightly smaller RMSEs compared to the ABA, except for the larch and other broadleaves where the RMSEs were similar for both approaches. The largest systematic errors occurred in the ITC approach, caused by non-detected trees. Although all delineated crown segments were used for the volume modeling, a large underprediction due to omission errors of the ITC delineation still appeared in the ITC approach, mainly due to the forest structure [14]. The semi-ITC approach underpredicted all volumes, except for the Norway spruce volume, which was negligibly overpredicted. Even though, the semi-ITC is compensating the problem related to the omission error, it is not able to eliminate it completely. On average, the species-specific volumes were achieved with the smallest systematic errors with the semi-ITC approach. The ABA approach also underpredicted all volumes, but overpredicted the Norway spruce and silver fir volumes. The overprediction in ABA can be the result of species

presence of the nearest sample plots. As the volumes were predicted based on selected nearest neighbors, the *k*MSN method can predict small volumes for tree species classes that do not really occur in a sample plot. Since the *k*NN method was used, the predicted values will have a smaller range than the observed because of an averaging effect, which can caused the underprediction for the ABA and semi-ITC approach. We have to consider that the systematic error of the semi-ITC approach is the result of the combination of the delineation and *k*NN method's characteristics. In most cases, the systematic errors obtained with the semi-ITC approach were smaller compared to the ABA. A similar observation was also found in the study of Breidenbach et al. [37].

In the literature, there are no similar studies comparing the species-specific attributes obtained by the ITC and semi-ITC approaches, except for Ørka et al. [23]. In general, the main problem of the ITC methods is the quite large omission error, caused by undetected understory and suppressed trees [59], mostly resulting in underprediction [12] of biophysical attributes when aggregated at the plot level [60]. This systematic error can be considerably reduced with the semi-ITC approach as demonstrated in our study. Comparing the semi-ITC and ABA inventory approaches, Breidenbach et al. and Rahlf et al. [37,61] showed that the semi-ITC approach provided prediction accuracies that were higher or similar to the ABA, while in the study of Ørka et al. [23], the ABA performed better than the semi-ITC approach. Based on a trade-off between the goodness of fit and the systematic error, the compared total and species-specific results suggest that the semi-ITC approach in total outperformed the other approaches.

For the *k*NN methods, a sufficient number of sample plots is required for the ABA in order to have a sufficient number of neighbors available for the calculation of the distance matrix. For example, 300–500 sample plots are usually applied in operational forest inventories. On the other hand, many studies showed that nonparametric models were in line with parametric models also with a lower number of observations (e.g., 200 sample plots) [44,62]. However, we assumed that 94 subsample plots using three nearest neighbors were sufficient to achieve good results. The reason to not apply a parametric method was that the field-observed species-specific volumes contained many values close to zero or zeros due to the absence of minority tree species in the sample plots. Moreover, in complex stands with a wide variety of tree sizes and species, the nonparametric methods might be preferred to avoid implausible (e.g., negative) predictions and to obtain a reasonable extrapolation beyond the range of calibration data. In fact, among the nonparametric methods, the *k*NN, in particular the *k*MSN method, have been shown to be efficient in providing simultaneous multivariate predictions at a satisfactory accuracy level [17,37,54,63,64].

The volumes of the minor species were always predicted with smaller accuracies than the volumes of the majority species. The reason could be the small share of some tree species, especially broadleaves, and thus it was difficult to obtain accurate results. Moreover, a large share of only one species is the typical situation of the European forests. This phenomenon of small accuracy of the minor species is typical also for other studies [23,37], but despite the small RMSEs, the information on the existence of the minority species in stands can be valuable information, for example in tree-oriented silvicultural practices. Looking at the problem from an economical perspective, minority species are of secondary interest as the majority of the harvested volume is coming from Norway spruce and larch. Other species are mainly used for energy wood, as is the case of the broadleaves volume, or for very specific uses (e.g., high quality furniture). Minority species are important from the ecological perspective and thus, the use of ITC or semi-ITCs approaches is essential in this case as it is difficult to monitor such species with the ABA approach [23]. The ITC and semi-ITC approaches can also be used to detect and report the presence and spread of non-native invasive species that can irreversibly alter the productivity of the systems they invade. The semi-ITC approach is overall quite good for predicting volumes of the minority and majority species. However, in studies where the volume of majority species is of high interest, the ABA is recommended, as the field data collection (e.g., tree positions) is less demanding and less costly compared to what is required for the semi-ITC approach.

5. Conclusions

The ITC approach reached high accuracies for the volumes of minority species but in general large systematic errors and the ABA approach resulted in small systematic errors and relatively high accuracies for the dominant species. Considering the systematic errors and accuracies for the total and species-specific volumes, the semi-ITC approach achieved the greatest balance. Eventually, we found that the ITC approach is important for applications in which information on the minority species is needed, such as for biodiversity studies and silviculture treatments. The ABA is recommended where the dominant species are a key value for management purposes, due to a less demanding collection of field data, relatively high accuracy, and minor systematic error for the dominant species. Overall, the semi-ITC approach has the potential to become competitive with the ABA, as it achieved more accurate results with negligible systematic error for the dominant species. Additionally, when the minor species volumes are requested, the semi-ITC approach might be preferred over the ITC approach as it resulted in small differences with the field measured values. In addition, when the ITC or semi-ITC approaches are applied, they could always be supplemented with the results of the ABA as its computation time is fast. We also suggest selecting the approach according to the application's tolerance to systematic errors. To conclude, the results of the semi-ITC approach are promising in providing accurate total and species-specific volumes. Further studies are needed to examine the accuracies of such an approach for other biophysical attributes and its use at the operational level over larger areas.

Acknowledgments: This work was mainly supported by the Edmund Mach Foundation. The acquisition of the remote sensing data and the collection of part of the field data were funded by the European Commission (project Alpine Space 2-3-2-FR NEWFOR) within the European Territorial Cooperation program "Alpine Space." This work was also partially supported by the hyperBio project (project 244599), financed by the BIONÆR program of the Research Council of Norway and TerraTec AS, Norway.

Author Contributions: K.K. as the main author processed the remote sensing data, performed the experiments and data analysis, and wrote the manuscript. K.K., M.D., and H.O.Ø. conceived and designed the experiments. L.F. planned, collected, and prepared the field data. M.D. and H.O.Ø. supervised and advised all the research work that led to this paper. M.D., H.O.Ø, and E.N. reviewed the manuscript and conducted the English editing.

Conflicts of Interest: The authors declare no conflict of interest.

References

1. Scrinzi, G.; Galvagni, D.; Marzullo, L. *I Nuovi Modelli Dendrometrici Per La Stima Delle Masse Assestamentali in Provincia di Trento*; Provincia Autonoma di Trento-Servizio Foreste e Fauna: Trento, Italy, 2010.
2. Næsset, E.; Gobakken, T.; Holmgren, J.; Hyyppä, H.; Hyyppä, J.; Maltamo, M.; Nilsson, M.; Olsson, H.; Persson, Å.; Söderman, U. Laser scanning of forest resources: The nordic experience. *Scand. J. For. Res.* **2004**, *19*, 482–499. [CrossRef]
3. Tomppo, E. The Finish multi-Source National Forest Inventory-Small area estimation and map production. In *Forest Inventory: Methodology and Applications*; Managing Forest Ecosystems; Kangas, A., Maltamo, M., Eds.; Springer: Dordrecht, The Netherlands, 2006; Volume 10, pp. 195–224.
4. Eid, T.; Gobakken, T.; Næsset, E. Comparing stand inventories for large areas based on photo-Interpretation and laser scanning by means of cost-Plus-Loss analyses. *Scand. J. For. Res.* **2004**, *19*, 512–523. [CrossRef]
5. Holmgren, J.; Persson, Å. Identifying species of individual trees using airborne laser scanner. *Remote Sens. Environ.* **2004**, *90*, 415–423. [CrossRef]
6. Dalponte, M.; Bruzzone, L.; Gianelle, D. Tree species classification in the southern Alps based on the fusion of very high geometrical resolution multispectral/hyperspectral images and LiDAR data. *Remote Sens. Environ.* **2012**, *123*, 258–270. [CrossRef]
7. Baltsavias, E.P. Airborne laser scanning: Basic relations and formulas. *ISPRS J. Photogramm. Remote Sens.* **1999**, *54*, 199–214. [CrossRef]
8. Wehr, A.; Lohr, U. Airborne laser scanning–An introduction and overview. *ISPRS J. Photogramm. Remote Sens.* **1999**, *54*, 68–82. [CrossRef]
9. Næsset, E. Predicting forest stand characteristics with airborne scanning laser using a practical two-Stage procedure and field data. *Remote Sens. Environ.* **2002**, *80*, 88–99. [CrossRef]

10. Popescu, S.C.; Wynne, R.H.; Nelson, R.F. Estimating plot-Level tree heights with lidar: Local filtering with a canopy-Height based variable window size. *Comput. Electron. Agric.* **2002**, *37*, 71–95. [CrossRef]
11. Maltamo, M.; Suvanto, A.; Packalén, P. Comparison of basal area and stem frequency diameter distribution modelling using airborne laser scanner data and calibration estimation. *For. Ecol. Manag.* **2007**, *247*, 26–34. [CrossRef]
12. Peuhkurinen, J.; Mehtätalo, L.; Maltamo, M. Comparing individual tree detection and the area-based statistical approach for the retrieval of forest stand characteristics using airborne laser scanning in Scots pine stands. *Can. J. For. Res.* **2011**, *41*, 583–598. [CrossRef]
13. Vauhkonen, J.; Ene, L.; Gupta, S.; Heinzel, J.; Holmgren, J.; Pitkanen, J.; Solberg, S.; Wang, Y.; Weinacker, H.; Hauglin, K.M.; et al. Comparative testing of single-tree detection algorithms under different types of forest. *Forestry* **2011**, *85*, 27–40. [CrossRef]
14. Kandare, K.; Ørka, H.O.; Chan, J.C.; Dalponte, M. Effects of forest structure and airborne laser scanning point cloud density on 3D delineation of individual tree crowns. *Eur. J. Remote Sens.* **2016**, *49*, 337–359. [CrossRef]
15. Ørka, H.O.; Næsset, E.; Bollandsås, O.M. Classifying species of individual trees by intensity and structure features derived from airborne laser scanner data. *Remote Sens. Environ.* **2009**, *113*, 1163–1174. [CrossRef]
16. Packalén, P.; Maltamo, M. Predicting the plot volume by tree species using airborne laser scanning and aerial photographs. *For. Sci.* **2006**, *52*, 611–622.
17. Packalén, P.; Maltamo, M. The k-MSN method for the prediction of species-specific stand attributes using airborne laser scanning and aerial photographs. *Remote Sens. Environ.* **2007**, *109*, 328–341. [CrossRef]
18. Niska, H.; Skon, J.-P.; Packalen, P.; Tokola, T.; Maltamo, M.; Kolehmainen, M. Neural networks for the prediction of species-Specific plot volumes using airborne laser scanning and aerial photographs. *IEEE Trans. Geosci. Remote Sens.* **2010**, *48*, 1076–1085. [CrossRef]
19. Popescu, S.C.; Wynne, R.H.; Scrivani, J.A. Fusion of small-Footprint lidar and multispectral data to estimate plot-Level volume and biomass in deciduous and pine forests in Virginia, USA. *For. Sci.* **2004**, *50*, 551–565.
20. Tonolli, S.; Dalponte, M.; Neteler, M.; Rodeghiero, M.; Vescovo, L.; Gianelle, D. Fusion of airborne LiDAR and satellite multispectral data for the estimation of timber volume in the Southern Alps. *Remote Sens. Environ.* **2011**, *115*, 2486–2498. [CrossRef]
21. Dalponte, M.; Ørka, H.O.; Gobakken, T.; Gianelle, D.; Næsset, E. Tree species classification in boreal forests with hyperspectral data. *IEEE Trans. Geosci. Remote Sens.* **2013**, *51*, 2632–2645. [CrossRef]
22. Hill, R.A.; Thomson, A.G. Mapping woodland species composition and structure using airborne spectral and LiDAR data. *Int. J. Remote Sens.* **2005**, *26*, 3763–3779. [CrossRef]
23. Ørka, H.O.; Dalponte, M.; Gobakken, T.; Næsset, E.; Ene, L.T. Characterizing forest species composition using multiple remote sensing data sources and inventory approaches. *Scand. J. For. Res.* **2013**, *28*, 677–688. [CrossRef]
24. Sarrazin, M.J.D.; Van Aardt, J.A.N.; Asner, G.P.; Mcglinchy, J.; Messinger, D.W.; Wu, J. Fusing small-Footprint waveform LiDAR and hyper spectral data for canopy-Level species classification and herbaceous biomass modeling in savanna ecosystems. *Can. J. Remote Sens.* **2011**, *37*, 653–665. [CrossRef]
25. Ahokas, E.; Hyyppä, J.; Yu, X.; Liang, X.; Matikainen, L.; Karila, K.; Litkey, P.; Kukko, A.; Jaakkola, A.; Kaartinen, H.; et al. Towards automatic single-Sensor mapping by multispectral airborne laser scanning. *Int. Arch. Photogramm. Remote Sens. Spat. Inf. Sci.* **2016**, *41*, 155–162. [CrossRef]
26. Yu, X.; Hyyppä, J.; Litkey, P.; Kaartinen, H.; Vastaranta, M.; Holopainen, M. Single-Sensor Solution to Tree Species Classification Using Multispectral Airborne Laser Scanning. *Remote Sens.* **2017**, *9*, 108. [CrossRef]
27. Junttila, S.; Kaasalainen, S.; Vastaranta, M.; Hakala, T.; Nevalainen, O.; Holopainen, M. Investigating bi-temporal hyperspectral lidar measurements from declined trees-Experiences from laboratory test. *Remote Sens.* **2015**, *7*, 13863–13877. [CrossRef]
28. Clark, M.L.; Roberts, D.A.; Clark, D.B. Hyperspectral discrimination of tropical rain forest tree species at leaf to crown scales. *Remote Sens. Environ.* **2005**, *96*, 375–398. [CrossRef]
29. Ferreira, M.P.; Zortea, M.; Zanotta, D.C.; Shimabukuro, Y.E.; De Souza Filho, C.R. Mapping tree species in tropical seasonal semi-Deciduous forests with hyperspectral and multispectral data. *Remote Sens. Environ.* **2016**, *179*, 66–78. [CrossRef]
30. Asner, G.P.; Knapp, D.E.; Boardman, J.; Green, R.O.; Kennedy-Bowdoin, T.; Eastwood, M.; Martin, R.E.; Anderson, C.; Field, C.B. Carnegie Airborne Observatory-2: Increasing science data dimensionality via high-Fidelity multi-Sensor fusion. *Remote Sens. Environ.* **2012**, *124*, 454–465. [CrossRef]

31. Luo, S.; Wang, C.; Xi, X.; Pan, F.; Peng, D.; Zou, J.; Nie, S.; Qin, H. Fusion of airborne LiDAR data and hyperspectral imagery for aboveground and belowground forest biomass estimation. *Ecol. Indic.* **2017**, *73*, 378–387. [CrossRef]
32. Næsset, E. Estimating timber volume of forest stands using airborne laser scanner data. *Remote Sens. Environ.* **1997**, *61*, 246–253. [CrossRef]
33. Hyyppä, J.; Inkinen, M. Detecting and estimating attributes for single trees using laser scanner. *Photogramm. J. Finl.* **1999**, *16*, 27–42.
34. Wang, Y.; Hyyppä, J.; Liang, X.; Kaartinen, H.; Yu, X.; Lindberg, E.; Holmgren, J.; Qin, Y.; Mallet, C.; Ferraz, A.; et al. International benchmarking of the individual tree detection methods for modeling 3-D canopy structure for silviculture and forest ecology using airborne laser scanning. *IEEE Trans. Geosci. Remote Sens.* **2016**, *54*, 5011–5027. [CrossRef]
35. Hyyppä, J.; Kelle, O.; Lehikoinen, M.; Inkinen, M. A segmentation-Based method to retrieve stem volume estimates from 3-D tree height models produced by laser scanners. *IEEE Trans. Geosci. Remote Sens.* **2001**, *39*, 969–975. [CrossRef]
36. Persson, Å.; Holmgren, J.; Soderman, U. Detecting and measuring individual trees using an airborne laser scanner. *Photogramm. Eng. Remote Sens.* **2002**, *68*, 925–932.
37. Breidenbach, J.; Næsset, E.; Lien, V.; Gobakken, T.; Solberg, S. Prediction of species specific forest inventory attributes using a nonparametric semi-Individual tree crown approach based on fused airborne laser scanning and multispectral data. *Remote Sens. Environ.* **2010**, *114*, 911–924. [CrossRef]
38. Vauhkonen, J.; Seppänen, A.; Packalén, P.; Tokola, T. Improving species-Specific plot volume estimates based on airborne laser scanning and image data using alpha shape metrics and balanced field data. *Remote Sens. Environ.* **2012**, *124*, 534–541. [CrossRef]
39. Moeur, M.; Stage, A.R. Most similar neighbor: An improved sampling inference procedure for natural resource planning. *For. Sci.* **1995**, *41*, 337–359.
40. Ørka, H.O.; Gobakken, T.; Næsset, E.; Ene, L.; Lien, V. Simultaneously acquired airborne laser scanning and multispectral imagery for individual tree species identification. *Can. J. Remote Sens.* **2012**, *38*, 125–138. [CrossRef]
41. McRoberts, R.; Nelson, M.; Wendt, D. Stratified estimation of forest area using satellite imagery, inventory data, and the k-Nearest Neighbors technique. *Remote Sens. Environ.* **2002**, *82*, 457–468. [CrossRef]
42. Yu, B.; Ostland, I.M.; Gong, P.; Pu, R.L. Penalized discriminant analysis of in situ hyperspectral data for conifer species recognition. *IEEE Trans. Geosci. Remote Sens.* **1999**, *37*, 2569–2577. [CrossRef]
43. Falkowski, M.J.; Hudak, A.T.; Crookston, N.L.; Gessler, P.E.; Uebler, E.H.; Smith, A.M.S. Landscape-Scale parameterization of a tree-Level forest growth model: A k-Nearest neighbor imputation approach incorporating LiDAR data. *Can. J. For. Res.* **2010**, *40*, 184–199. [CrossRef]
44. Pippuri, I.; Maltamo, M.; Packalen, P.; Mäkitalo, J. Predicting species-Specific basal areas in urban forests using airborne laser scanning and existing stand register data. *Eur. J. For. Res.* **2013**, *132*, 999–1012. [CrossRef]
45. Räty, J.; Vauhkonen, J.; Maltamo, M.; Tokola, T. On the potential to predetermine dominant tree species based on sparse-Density airborne laser scanning data for improving subsequent predictions of species-Specific timber volumes. *For. Ecosyst.* **2016**, *3*, 1–17. [CrossRef]
46. R Development Core Team R: A Language and Environment for Statistical Computing. Available online: http://www.r-project.org (accessed on 22 September 2016).
47. Kaartinen, H.; Hyyppä, J.; Yu, X.; Vastaranta, M.; Hyyppä, H.; Kukko, A.; Holopainen, M.; Heipke, C.; Hirschmugl, M.; Morsdorf, F.; et al. An international comparison of individual tree detection and extraction using airborne laser scanning. *Remote Sens.* **2012**, *4*, 950–974. [CrossRef]
48. Karatzoglou, A.; Smola, A.; Hornik, K. The Kernlab Package. Available online: https://cran.r-project.org/web/packages/kernlab/index.html (accessed on 16 February 2017).
49. Dalponte, M.; Coomes, D.A. Tree-Centric mapping of forest carbon density from airborne laser scanning and hyperspectral data. *Methods Ecol. Evol.* **2016**, *7*, 1236–1245. [CrossRef]
50. Crookston, N.L.; Finley, A.O. YaImpute: An R Package for kNN Imputation. *J. Stat. Softw.* **2008**, *23*, 1–16. [CrossRef]
51. McRoberts, R.E.; Gobakken, T.; Næsset, E. Post-Stratified estimation of forest area and growing stock volume using lidar-Based stratifications. *Remote Sens. Environ.* **2012**, *125*, 157–166. [CrossRef]

52. Nilsson, M. Estimation of tree heights and stand volume using an airborne lidar system. *Remote Sens. Environ.* **1996**, *56*, 1–7. [CrossRef]
53. Mohammadi, J.; Joibary, S.S.; Yaghmaee, F.; Mahiny, A.S. Modelling forest stand volume and tree density using Landsat ETM+data. *Int. J. Remote Sens.* **2010**, *31*, 2959–2975. [CrossRef]
54. Mäkelä, H.; Pekkarinen, A. Estimation of forest stand volumes by Landsat TM imagery and stand-Level field-Inventory data. *For. Ecol. Manag.* **2004**, *196*, 245–255. [CrossRef]
55. Packalén, P.; Temesgen, H.; Maltamo, M. Variable selection strategies for nearest neighbor imputation methods used in remote sensing based forest inventory. *Can. J. Remote Sens.* **2012**, *38*, 557–569. [CrossRef]
56. Packalén, P.; Suvanto, A.; Maltamo, M. A two stage method to estimate species-specific growing stock. *Photogramm. Eng. Remote Sens.* **2009**, *75*, 1451–1460. [CrossRef]
57. Puliti, S.; Gobakken, T.; Ørka, H.O.; Næsset, E. Assessing 3D point clouds from aerial photographs for species-Specific forest inventories. *Scand. J. For. Res.* **2017**, *32*, 68–79. [CrossRef]
58. Wikström, P.; Edenius, L.; Elfving, B.; Eriksson, L.O.; LäMåS, T.; Sonesson, J.; ÖHMAN, K.; Wallerman, J.; Waller, C.; Klintebäck, F. The Heureka forestry decision support system: An overview. *Math. Comput. For. Nat. Sci.* **2011**, *3*, 87–95.
59. Latifi, H.; Fassnacht, F.E.; Müller, J.; Tharani, A.; Dech, S.; Heurich, M. Forest inventories by LiDAR data: A comparison of single tree segmentation and metric-Based methods for inventories of a heterogeneous temperate forest. *Int. J. Appl. Earth Obs. Geoinf.* **2015**, *42*, 162–174. [CrossRef]
60. Yu, X.; Hyyppä, J.; Holopainen, M.; Vastaranta, M. Comparison of area-Based and individual tree-Based methods for predicting plot-Level forest attributes. *Remote Sens.* **2010**, *2*, 1481–1495. [CrossRef]
61. Rahlf, J.; Breidenbach, J.; Solberg, S.; Astrup, R. Forest parameter prediction using an image-Based point cloud: A comparison of semi-ITC with ABA. *Forests* **2015**, *6*, 4059–4071. [CrossRef]
62. Bollandsås, O.M.; Maltamo, M.; Gobakken, T.; Næsset, E. Comparing parametric and non-Parametric modelling of diameter distributions on independent data using airborne laser scanning in a boreal conifer forest. *Forestry* **2013**, *86*, 493–501. [CrossRef]
63. Hudak, A.T.; Crookston, N.L.; Evans, J.S.; Hall, D.E.; Falkowski, M.J. Nearest neighbor imputation of species-Level, plot-Scale forest structure attributes from LiDAR data. *Remote Sens. Environ.* **2008**, *112*, 2232–2245. [CrossRef]
64. Penner, M.; Pitt, D.G.; Woods, M.E. Parametric vs. nonparametric LiDAR models for operational forest inventory in boreal Ontario. *Can. J. Remote Sens.* **2013**, *39*, 426–443.